International Journal of Advanced Culture Technology Vol.10 No.4 470-477 (2022)
DOI https://doi.org/10.17703/IJACT.2022.10.4.470

IJACT 22-12-56

Study on Design of Two-Axis Image Stabilization Controller through Drone Flight Test Data Standardization

[1]Jeongwon Kim, [2]Gyuchan Lee, [3]Dong-gi Kwag*

[1,2]Dept. of Aeronautical System Engineering, Hanseo Univ., Korea
[3]Prof., Dept. of Aero Mechanical Engineering, Hanseo Univ., Korea*
dnjs3924@naver.com, dlrbcks9980@naver.com, dgkwag@hanseo.ac.kr

Abstract

EOTS for drones is showing another aspect of market expansion in detection and recognition areas previously occupied by artificial satellites. The two-axis EOTS for drones controls the vibration or disturbance caused by the drone during the mission so that EOTS can accurately recognize the goal. Vibration generated by drones is transmitted to EOTS. Therefore, it is essential to develop a stabilization controller that attenuates vibrations transmitted from drones so that EOTS can maintain the viewing angle. Therefore, it is necessary to standardize drone disturbance and secure the performance of EOTS disturbance attenuation controller optimized for disturbance level through this. In this paper, a method of standardizing drone disturbance applied to EOTS is studied, through which EOTS controller simulation is performed and stabilization controller shape is selected and designed.

Keywords: *EOTS, Disturbance, Power Spectral Density, Standardization, Controller Type*

1. INTRODUCTION

With increasing diversity of the utilization and missions of drones, the success of drone missions is directly related to the performance of the electro-optical targeting system (EOTS) mounted on drones. EOTS transmits images and target information to fire control systems by searching, detecting, and tracing targets [1]. With the advent of the fourth industrial revolution, EOTS has emerged as an important technology in the field of detection and recognition, which is one of the core technologies of drones. In South Korea, many companies have joined the field of defense and space technology, and EOTS development has been performed in a wide range, including the protection of marine vessels and wheel-type anti-aircraft artillery. For drones, however, there are still a relatively small amount of patent applications for EOTS in Korea.

The performance of EOTS is an indicator for tracing the target accurately by attenuating the disturbance transmitted from the drone as much as possible. To secure the performance, it is necessary to analyze the disturbance of various drones in the frequency band. If the analyzed drone disturbance level is standardized and applied to various EOTS controllers to be designed, a controller type favorable for line-of-sight (LOS) stabilization can be selected.

In this study, the disturbance generated from a drone is acquired by installing a dummy and a MEMS IMU

Manuscript received: November 24, 2022 / revised: November 30, 2022 / accepted: December 9, 2022
Corresponding Author: dgkwag@hanseo.ac.kr
Tel: +82-041-671-6255
Dept. Aero Mechanical Engineering, Hanseo University, Korea

sensor on an actual drone, and an environment applicable to EOTS simulation is constructed. Research is also conducted on disturbance standardization for the design of LOS stabilization controllers and EOTS disturbance robustness.

2. MAIN BODY

2.1 Drone disturbance acquisition

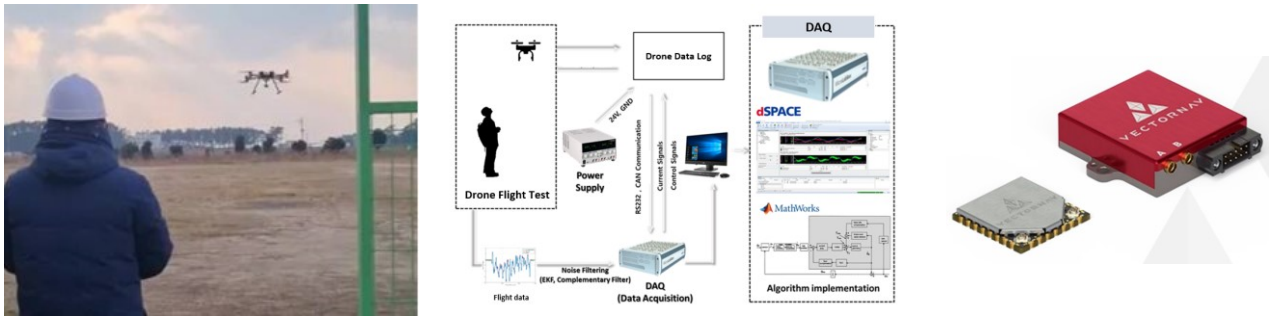

Figure 1. Drone Data Acquisition, Configuration diagram and Sensors

To standardize the disturbance data coming from drones, disturbance was acquired by flying an actual drone. In this instance, a MEMS IMU sensor was installed at the bottom of the drone, and a 2kg EOTS dummy was also installed to increase the reliability of disturbance data acquisition. Data acquisition was performed twice at each reference height (5, 25, 50, 75, and 100 m).

As a representative case, the disturbance acquired during flight at an altitude of 5 m included the pan direction (yaw) and tilt direction (pitch) with respect to the rotation angle of two-axis EOTS as well as the angular velocity (rad/sec) in the roll direction. Figure 2 shows the raw data of the acquired disturbance.

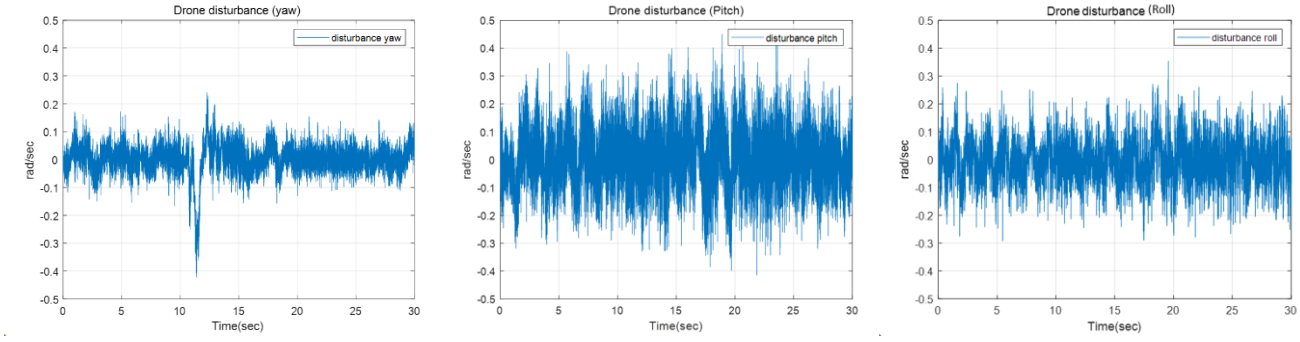

Figure 2. 3-Axis Drone Disturbance

2.2 Disturbance standardization

The disturbance acquired from the drone was standardized. Disturbance standardization must be performed for the following reasons. Since the disturbance applied to a drone during flight is significantly affected by an unexpected gust or a specific situation, it is necessary to acquire disturbance under various conditions to develop a more precise stabilization system. In this instance, the application of disturbance under various conditions to the stabilization control system requires considerable time and manpower, and it is not easy to establish a criterion for selecting appropriate disturbance. If random vibration is created using simulation and

it is used to avoid these problems, there is a difference from environmental disturbance that affects the actual drone and EOTS. Therefore, appropriate disturbance that affects drones and EOTS is created by performing disturbance standardization after acquiring various actual disturbances. The goal of disturbance standardization is to artificially apply disturbance in real time to the actual EOTS motor so that the EOTS stabilization algorithm system can be researched more efficiently.

First, power spectral density (PSD) analysis is conducted on the disturbance. PSD analysis is a method of expressing the magnitude of a signal by frequency in the unit of $\mathrm{PowerRMS}^2/Hz$ on a log scale graph by representing it as a mean square. In other words, it shows the strength of the signal according to the frequency as a frequency function.

The acquired data are subjected to frequency analysis from 0 to 100 Hz. For the data, the bandwidth is divided according to a certain rule and the average magnitude of the signal is prepared for each section. As for the bandwidth section selection criterion, the 3/4 point (75 Hz) of the reference frequency range (0 to 100 Hz) was selected, and the 3/4 point (56.25 Hz) of the remaining frequency range (0 to 75 Hz) was selected. This was repeated until 0.1 Hz was selected. This method makes it easy to analyze disturbance characteristics at low frequencies because the frequency can be divided in more detail in the low-frequency zone (0 to 1 Hz).

For each selected frequency, the power value of the raw data of each axis acquired is replaced with the average and summarized. As shown in Eq. 1, the range for each selected frequency is expressed as a bandwidth, and a representative frequency is selected.

$$Representative\ Frequency_n = \frac{Selected\ Frequency_n + Selected\ Frequency_{n-1}}{2}$$

$$Bandwidth_n = Selected\ Frequency_n - Selected\ Frequency_{n-1} \qquad \text{Eq. 1}$$

For example, the selected frequency and bandwidth for the yaw-axis disturbance and the subsequent power value are summarized in Table 1.

The peak value at each frequency level is derived from the averaged power value. Eq. 2 is the equation to derive the peak value at each frequency.

$$\begin{aligned} Averaged\ Power\ Value \times Bandwidth[Hz] &= \left(A(\mathrm{rad/sec})(RMS)\right)^2 \\ \sqrt{\left(A(\mathrm{rad/sec})(RMS)\right)^2} &= A(rad/sec)(RMS) \\ A(\mathrm{rad/sec})(RMS) \times \sqrt{2} &= A_n(\mathrm{rad/sec}) = A_n[Peak] \end{aligned} \qquad \text{Eq.2}$$

The obtained peak values are then substituted for each frequency to create a standardized disturbance signal. Eq. 3 is the equation to create the standardized disturbance signal (S). In this instance, a random phase difference is applied when a sine function is created at each frequency. This method makes it possible to apply disturbance in various shapes to simulation because it is possible to acquire standardized disturbance in various shapes at the same level.

$$\begin{gathered} a_n = Sine\ Signal\ for\ Each\ Frequency, \qquad A_n = Amplitude\ [Peak] \\ \omega_n = Representative\ Frequency[Hz], \qquad c_n = Random\ Phase\ (0{\sim}360\ deg) \\ a_n = A_n \cdot sin\ sin\ (\omega_n t \cdot 2\pi + c_n) \qquad S = a_1 + a_2 + \cdots + a_n \end{gathered} \qquad \text{Eq. 3}$$

Table 1. Power Value by Representative Frequency

Selected Frequency [Hz]	Representative Frequency [Hz]	Bandwidth [Hz]	Averaged Power Value (((rad/sec)RMS)^2)/Hz
0	-	-	-
0.1	0.05	0.1	0.000314788
0.13	0.115	0.03	0.000789216
0.18	0.155	0.05	0.000412551
0.24	0.21	0.06	0.001833269
…	…	…	…
1	0.875	0.25	0.001449112
…	…	…	…
10.01	8.76	2.5	2.84012E-06
13.35	11.68	3.34	3.35689E-06
17.8	15.575	4.45	5.98566E-06
23.73	20.765	5.93	1.51075E-05
31.64	27.685	7.91	1.50416E-05
42.19	36.915	10.55	2.88575E-05
56.25	49.22	14.06	0.000520185
75	65.625	18.75	1.02517E-05
100	87.5	25	0.000230829

Table 2 shows the RMS levels of the raw disturbance transferred from the drone and the standardized disturbance. It can be seen that the RMS levels are almost identical. Figure 3 shows the standardized signal (S) for each axis as in Eq. 3.

Table 2. Effective Value Levels for Raw and Standardized data

Axis	Raw data [RMS]	Standardized data [RMS]
Yaw	0.0559	0.0554
Pitch	0.126	0.126
Roll	0.0841	0.0840

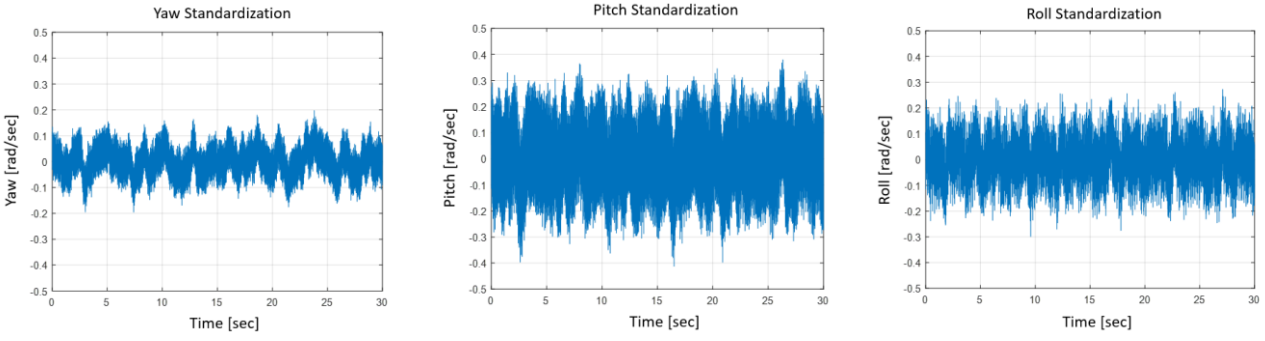

Figure 3. 3-Axis Standardized Drone Disturbance

Figure 4 shows the results of conducting PSD analysis and standardization on the disturbance acquired from each axis.

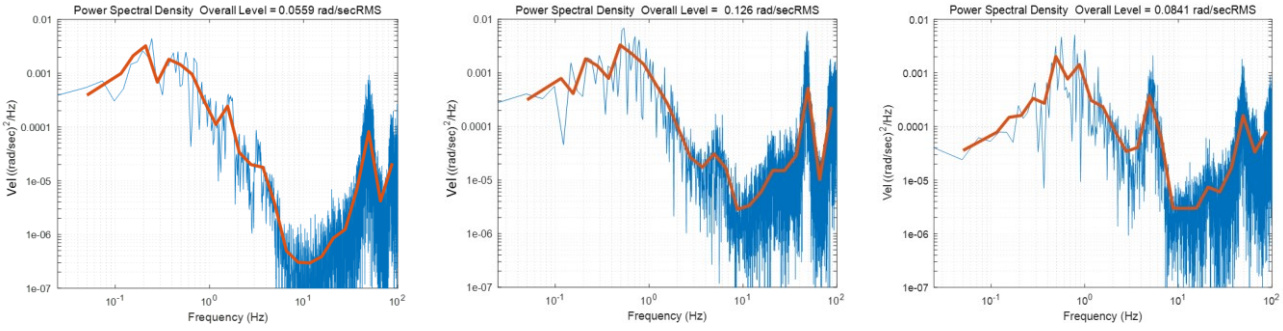

Figure 4. Power Spectral Density of Raw and Standardized data from 3-Axis

2.3 Frequency response according to the controller shape

It is not easy to compensate for nonlinear elements, such as friction, in the system because they are difficult to measure and predict accurately. Therefore, the plant is driven and controlled using an electric motor to reach the final target value [2]. The controllers commonly used for motor control include P control, PI control, and PI LEAD control. The control system can be expressed as a block diagram in Figure 5.

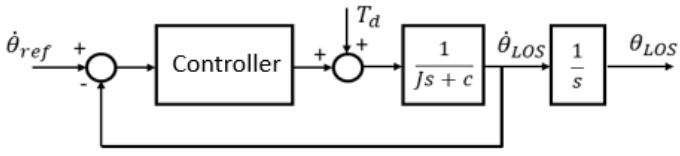

Figure 5. Block Diagram of Control System

In this instance, if the angle output for the disturbance is expressed as a transfer function in the control system, it can be expressed as θ_{LOS}/T_d. To examine the frequency response according to the controller shape, the controller can be summarized in five transfer function types as shown in Table 3.

Table 3. Shape of Transfer Function for Angular Output for Disturbance

Controller	θ_{LOS}/T_d
P	$\frac{N}{K_1 s^2 + K_2 s}$
PI	$\frac{N}{K_1 s^2 + K_2 s + K_3}$
PI(LPF)	$\frac{N_1 s}{K_1 s^3 + K_2 s^2 + K_3 s + K_4}$
PI LEAD	$\frac{N_1 s + N_2}{K_1 s^3 + K_2 s^2 + K_3 s + K_4}$
PI(LPF) LEAD	$\frac{N_1 s^2 + N_2 s}{K_1 s^4 + K_2 s^3 + K_3 s^2 + K_4 s + K_5}$

Figure 6 shows the frequency response according to the shape of the disturbance response transfer function.

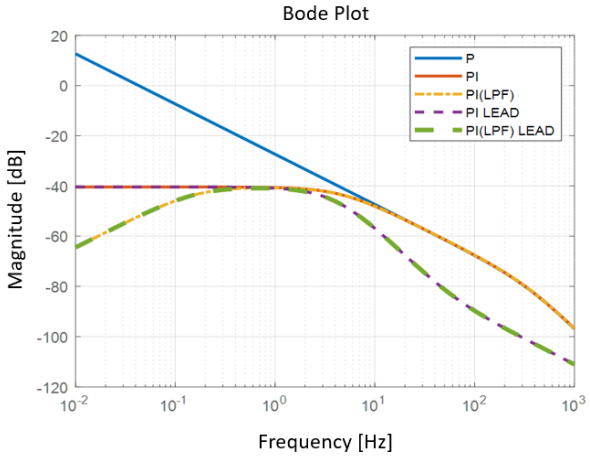

Figure 6. Frequency Response according to the Shape of the Disturbance Response Transfer Function

As can be seen from the figure, low-frequency disturbance attenuation characteristics are insufficient in the low-frequency response for P control (Type 1). For PI and PI LEAD control, low-frequency disturbance attenuation characteristics are moderate (Type 2). In the case of PI(LPF) and PI(LPF) LEAD control, low-frequency disturbance attenuation characteristics are excellent due to the application of the LowPass Filter (Type 3). Therefore, the system response under the application of disturbance was examined using the PI(LPF) LEAD controller.

2.4 Stabilization simulation disturbance response

It was examined whether a response close to the stabilization target was derived when the standardized disturbance was applied in EOTS stabilization simulation. In this instance, the rotation axis (two axes; Pan and Tilt) inertia values and motor friction for disturbance response simulation were derived through EOTS 3D modeling analysis and motor drive experiments. In the case of the friction model, a static friction model, Coulomb friction, and viscous friction typically affect control during motor drive [3]. Among them, static friction and viscous friction models for LOS stabilization control simulation were obtained through motor drive experiments and simulation.

First, the moment of inertia of each axis was obtained among EOTS dynamic characteristics. Its value was derived by applying a command to the gimbal motor and comparing the input torque and the angular velocity magnification factor. It was also compared with the moment of inertia that can be identified from 3D CAD modeling structural characteristics. The equation to derive the moment of inertia is expressed as Eq. 4.

$$\left|\frac{\dot{\theta}}{T_m}\right| = \left|\frac{1}{Js+c}\right| = \sqrt{\left(\frac{1}{j(J\omega)+c}\right)^2}, \quad \left|\frac{\dot{\theta}}{T_m}\right| \cong \frac{1}{Js} \rightarrow J = \frac{T_m}{\dot{\theta}\omega} \qquad \text{Eq. 4}$$

Friction is a phenomenon that occurs between two objects in contact. Owing to its very strong nonlinear characteristics and various environmental changes, it is difficult to obtain an accurate friction model. For EOTS, static friction (c_1) means friction that occurs between the balls and inner/outer rings of the bearing while they are not moving in contact. Viscous friction (c_2) is a type of linear friction, and it occurs as the friction caused by the oil inside the ball bearing. Static friction is measured by applying a current to the motor

in a low-frequency sawtooth waveform and observing the point at which the motor overcomes friction. The maximum current value at the point is observed by repeating this motor drive experiment, and it is used as static friction. The equation to obtain static friction is expressed as Eq. 5.

$$Static\ friction[Nm] = Torque\ constant\left[\frac{Nm}{A}\right] \cdot Friction\ Overcoming\ Current[\mathrm{A}] \quad \text{Eq. 5}$$

Since all dynamic characteristics, except for viscous friction, were obtained using Eqs. 4 and 5, viscous friction (c_2) was obtained by performing parameter estimation. Therefore, the configuration plot of the algorithm that applied dynamic characteristic modeling can be expressed as Figure 7, and it was applied to simulation.

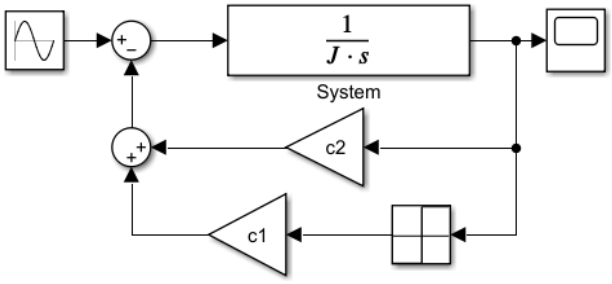

Figure 7. Dynamic Characteristic Modeling Configuration Plot

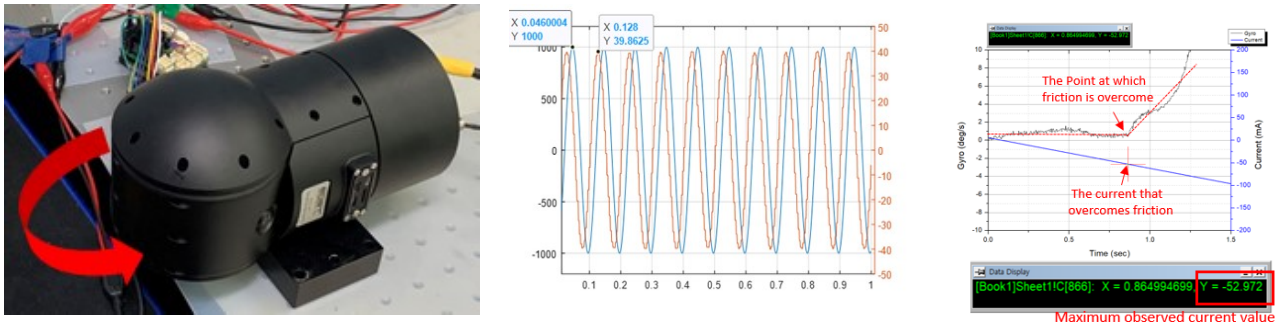

Figure 8. Dynamic Characteristics Experiment

Table 4. Dynamic Characteristics of EOTS

	Pan Axis	Tilt Axis
Inertia	0.001670 [kg.mm^2]	0.000622[kg.mm^2]
Static Friction	0.00144	0.00144
Viscous Friction	0.0017	0.0017

After applying appropriate P, I, and Lead gains to the control simulation algorithm that configured the dynamic characteristics of Table 4 as shown in Figure 4, the angle response (θ_{LOS}) was examined. The angle response of the disturbance that passed through the controller (θ_{LOS}) was obtained as shown in Figure 9, and its effective values can be seen in Table 5.

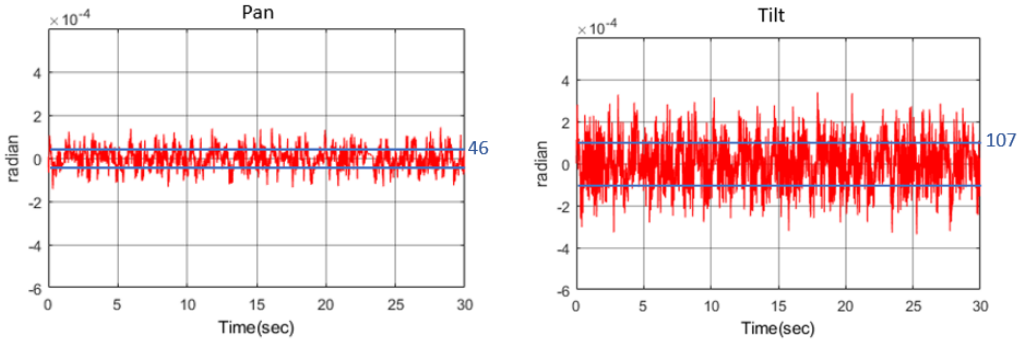

Figure 9. Disturbance Response of 2-Axis

Table 5. Effective Values of Disturbance Response

RMS	Pan Axis	Tilt Axis
μRad	46	107

3. CONCLUSION

The unbalanced random disturbance coming from a drone in flight was measured and standardized. The standardized disturbance is highly reliable at the same level as the actual flight data in simulation, and easily compatible with various electro-optical targeting system (EOTS) line-of-sight (LOS) stabilization controllers with various dynamic characteristics.

For LOS stabilization, a controller shape with high attenuation performance in low and high frequency bands, except for a specific frequency band, was selected. When the standardized flight disturbance data were applied to the algorithm and the angle response to the disturbance was examined, the disturbance attenuation performance and angle response of the controller could be confirmed. Through future research, disturbance data standardization will be applied to diversified EOTS development using the method presented in this study, and it will be used as an EOTS development index.

ACKNOWLEDGEMENT

This study was funded by the government of the Republic of Korea (Ministry of Trade, Industry and Energy and Defense Acquisition Program Administration) and funded by the Civil and Military Cooperation Promotion Agency. (Convention No. UD100044TU)

REFERENCES

[1] Sang-eun Lee, Hyung Gun Park, and Tae Won Lee, "A Study of the Mechanical Shock Response of an Image Sensor Unit in an Electro-Optical Targeting System Mounted on a Military Vehicle, *The Korean Society of Mechanical Engineers,* Vol. 42, No. 4, pp. 391-398, 2018

[2] Jin-bok Lee, Han –go Choi, "The Control for the 2-Axis Stabilized Gimbal using the PI-LEAD Algorithm," *The Korea institute of convergence signal processing*, Vol. 14, No. 2 pp. 117-123, 2013

[3] Byoung Ju Lee, Gwang Tae Kim, Hong Cheol Kim, and Young June Sine, "Static and Dynamic Friction Analysis of Actuation Module for Friction Compensation of Exoskeleton Robot," *Journal of the Korean Society for Rrecision Engineering,* Vol. 36, No. 10, pp. 929-935, October 2019